Lightweight Data-Driven Planning Method of Hybrid Energy Storage Systems in the New Power System

Yanda Huo, Jiahui Yang, *Student Member, IEEE*, Jiahui Qu, Chao Zhang, Li Zhou, Weiran Zhao, Hua Jiang, Zhen Wu, Jianfeng Dai, Wei Duan, Jintao Jiang, and Chengshan Wang, *Senior Member, IEEE*

***Abstract*—With the development of energy storage systems (ESS), the integration of a hybrid energy storage system (HESS) in the new power system is beneficial to alleviate the uncertainty and inflexibility caused by the high penetration of renewable energy sources (RES). However, the multi-time scale coupling characteristics of HESS pose challenges to conventional planning methods in the modeling process. To improve the applicability of the planning model, a lightweight data-driven planning method with decoupled operation and planning stage is proposed in this paper. First, the demand function of the new power system is quantified for HESS based on the production simulation. Second, a graphical model is established to describe the multi-time scale characteristic of HESS. Then, considering the investment cost, a lightweight data-driven planning model is proposed to optimize the capacities of HESS, including energy-energy ESS and power-energy ESS. Finally, the proposed method is verified using a regional test case. Case studies show that average electricity cost of the proposed method is the lowest. In addition, the maximum 5-minute fluctuation is reduced by more than 50% due to power-energy ESS. Therefore, the proposed lightweight data-driven planning method for HESS can effectively solve the planning problems of HESS.**

***Index Terms*—Data-driven, energy-energy ESS, hybrid energy storage system (HESS), lightweight, power-energy ESS, renewable energy sources (RES).**

NOMENCLATURE

$P(t)$	the envelope curve of maximum power unbalance.
θ	the probability threshold.
$P'(t)$	the envelope curve of maximum power unbalance with uncertainty.
P_i	the power of ESS.
A_i	the capacity of ESS.
C_i	the investment cost per unit power-scale of energy-energy ESS.
$P^{\mathrm{RES}}(t)$	renewable energy output.
$P_{\lambda}^{\mathrm{IMF}}(t)$	the m order modal component of the IMF.
$P^{\mathrm{H}}(t)$	the high-frequency fluctuation information.
$P^{\mathrm{L}}(t)$	the low-frequency steady-state information.
$C^{\mathrm{ESS\_SC}}$	the investment cost coefficient for the power-energy ESS capacity.
$E^{\mathrm{ESS\_SC}}$	the configured capacity of the power-energy ESS.
$C^{\mathrm{OPER\_SC}}$	the operating cost coefficient for the power-energy ESS.
C^{B}	the opportunity compensation cost coefficient.
$P_{\mathrm{load}}[t]$	the total load at time t.
C_{gas}	the investment cost per unit of power generation capacity for the gas plant.
D_{gas}	the operating cost per unit of power generation capacity for the gas plant.
P_{gas}	the power of the gas plant.
Q_{gas}	the generation of the gas plant.
$\begin{Bmatrix} U\|u_1,u_2,\ldots, \\ u_m\ldots u_M \end{Bmatrix}$	the data set of uncertain parameters.

Received 16 August 2024; revised 14 November 2024; accepted 25 December 2024. Date of publication 17 February 2025; date of current version 21 May 2025. Paper 2024-ESC-0936.R1, presented at the 2023 IEEE/IAS Industrial and Commercial Power System Asia, Chongqing, China, Jul. 07–09, and approved for publication in the IEEE TRANSACTIONS ON INDUSTRY APPLICATIONS by the Energy Systems Committee of the IEEE Industry Applications Society [DOI: 10.1109/ICPSAsia58343.2023.10294895]. This work was supported by the Postdoctoral project through China Electric Power Planning & Engineering Institute. *(Yanda Huo and Jiahui Yang contributed equally to this work.) (Corresponding author: Jiahui Yang.)*

Yanda Huo, Chao Zhang, Li Zhou, Weiran Zhao, Hua Jiang, Zhen Wu, Jianfeng Dai, and Wei Duan are with the China Electric Power Planning & Engineering Institute, Beijing 100120, China (e-mail: ydhuo@eppei.com).

Jiahui Yang and Chengshan Wang are with the Key Laboratory of Smart Grid of Ministry of Education, Tianjin University, Tianjin 300072, China (e-mail: yjh@tju.edu.cn; cswang@tju.edu.cn).

Jiahui Qu is with State Grid Tangshan Power Supply Company, Tangshan 063000, China (e-mail: jhquuu@163.com).

Jintao Jiang is with State Grid Changchun Power Supply Company, Changchun 130000, China (e-mail: jjt8256@163.com).

Color versions of one or more figures in this article are available at https://doi.org/10.1109/TIA.2025.3542731.

Digital Object Identifier 10.1109/TIA.2025.3542731

I. INTRODUCTION

WITH the implementation of the action plan for carbon peaking and carbon neutrality, non-fossil energy consumption is increasing continually in China[1], [2]. Large-scale renewable energy sources have been integrated into the new power system, which has led to problems such as uncertainty, inflexibility [3], and the unbalance of power and energy with demands [4].

With the maturity of energy storage technology, energy storage systems (ESS) are widely deployed in the new power system as well as the industrial park to provide regulation resources. Ref. [5] introduced the potential and defects of grid-scale energy storage and put forward some views on the current service regulation and market design. The access of ESS in Ref. [6] effectively enhanced the frequency stability in the low-inertia power system. Ref. [7] verified the advantages of ESS as a

flexible resource to participate in the frequency regulation of the electricity auxiliary service market. Many studies on planning methods for ESS have been conducted. Ref. [8] proposed an ESS optimal planning and scheduling method for power system congestion management considering renewable energy. Ref. [9] presented a unified stochastic planning method for battery energy storage systems in power systems including wind power plants. Ref. [10] described a novel tri-level robust planning-operation co-optimization model to determine the capacity, power, location and scheduling strategy of distributed energy storage systems.

However, the traditional ESS with a single technical route is challenged by the diversified demand of the new power system. To match the energy storage demand on multi-time scales, a hybrid energy storage system (HESS) can be utilized [11]. HESS consists of a number of storage technologies based on chemical, mechanical, hydrogen, and thermal energy, which can satisfy the energy storage demand on a short-, mid-, and long-term time scale. In Ref. [12], a HESS using battery energy storage with superconducting magnetic energy storage was proposed to reduce battery cycling while smoothing power flow. Ref. [13] introduced a new joint control strategy for the HESS with battery and super-capacitor in a photovoltaic-based DC grid system. An operational optimization model for electric and thermal ESS was presented in Ref. [14], and the results show that HESS can significantly reduce operating costs compared to a single ESS. A two-stage stochastic programming model is proposed in Ref. [15], which focuses on the HESS planning problem to enhance the operational flexibility, including battery and thermal storage tank. In Ref. [16], an energy storage capacity expansion model is proposed for the integrated energy system to determine the size of the HESS consisting of the power type battery and capacity type battery. Ref. [17] proposed a planning method for HESS, in which the super-capacitor energy storage is configured on the substation side while the electrochemical energy storage is configured on the user side.

As the planning stage and the operation stage of ESS are coupled, conventional planning methods for HESS face three key challenges:

1) Traditional optimization methods mainly focus on configuring the total capacity and storage duration of the system. However, they often lack multi-time scale analysis of HESS, such as hourly, daily, weekly, and monthly scales.
2) In a new power system with high uncertainty, it is difficult to model across multiple time scales. Traditional optimization models usually rely on scenario clustering, which makes it challenging to comprehensively consider wind and solar load variations throughout the year.
3) The optimization problem's complexity increases due to the multi-time scale characteristics. The large number of integer variables in the optimization stage requires mixed-integer linear programming, which can be difficult to solve efficiently.

Therefore, establishing a coupling model for both planning and operation stages in HESS remains challenging. This paper aims to propose a versatile and lightweight data-driven planning method with decoupled operation and planning stages specifically for HESS, capable of handling multi-time scale dynamics, as shown in Fig. 1.

The main contributions of this study are summarized as follows:

1) Based on the data from the production simulation, the demand function of the power system is quantified. Considering the uncertainty of renewable energy and loads, the demand function is further modified based on Monte-Carlo simulation.
2) A graphical model is established to describe the multi-time scale characteristic of HESS. Then, a lightweight data-driven planning model with decoupled operation and planning stages is proposed to optimize the capacities of HESS, including energy-energy ESS and power-energy ESS.

The remainder of this paper is organized as follows. Section II introduces the quantification process of the demand function for HESS. In Section III, a graphical model and planning models are established to describe the multi-time scale characteristic of HESS. Then, a lightweight data-driven planning model with decoupled operation and planning stages is proposed. Case studies and verification are presented in Section IV. Section V presents the conclusions.

II. Quantitative Demand Analysis

Since the planning problem of HESS is the expansion planning problem of power systems, the power planning scheme can be used as the boundary condition. The operational states of the power planning scheme can be simulated by the mature production simulation software. Based on the operation data, the demand function of power systems could be quantified for HESS [15].

A. Demand Quantification of HESS

From the perspective of the new power system, the main steady-state operation demand can be described by the multi-time scale unbalance of power and energy, including peak shaving, seasonal energy regulation, etc. Based on the optimized operation data obtained from the production simulation, hourly power shortage of the new power system can be analyzed. Taking a typical day as an example, the power shortage in each hour can be illustrated as shown in Fig. 2.

To facilitate analysis, the power shortage of each hour is sorted according to its size, and its envelope curve $P(t)$ can be obtained by using the data fitting method as shown in Fig. 3. The function $P(t)$ represents the relationship between the power demand and time in the typical day. With function $P(t)$, the power demand of the typical day is quantified.

The analysis period can also be extended from a typical day to a planning year. The characteristics of each continuous period of power shortage can be statistically analyzed. A number of areas can be formed by the graphical representation of the power demand, as shown in Fig. 4. These graphical areas can also be normalized as shown in Fig. 5.

To quantify characteristics of power demand in the whole planning year, the above-mentioned areas can be stacked at $t =$

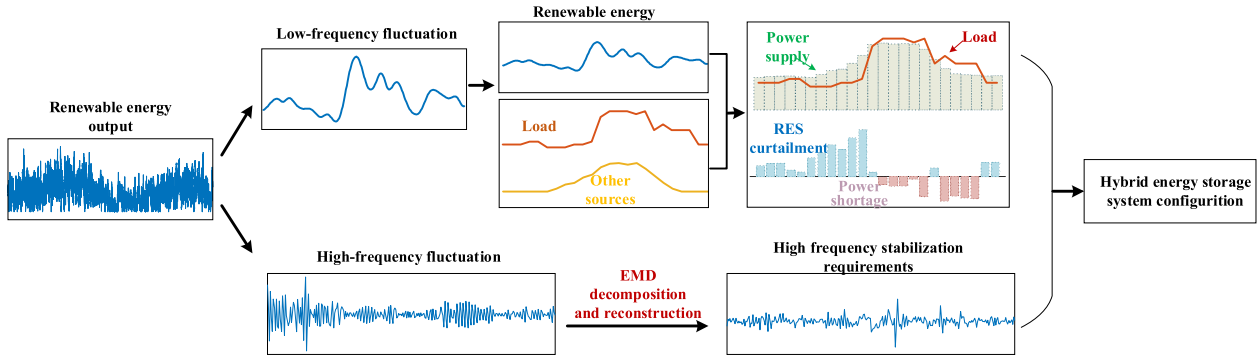

Fig. 1. Framework of the lightweight data-driven planning method for HESS.

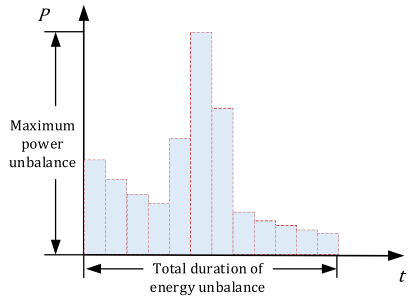

Fig. 2. The power unbalance on a typical day.

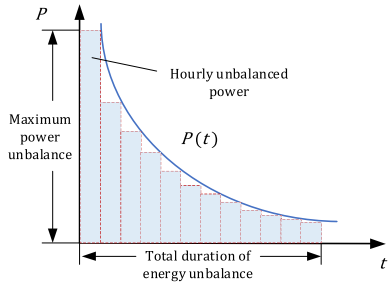

Fig. 3. The normalized power demand on a typical day.

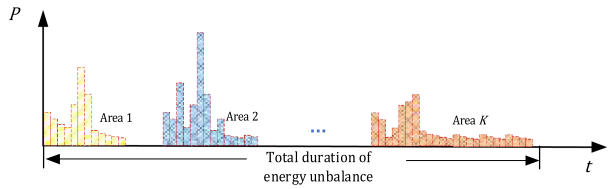

Fig. 4. The power unbalance in the planning year.

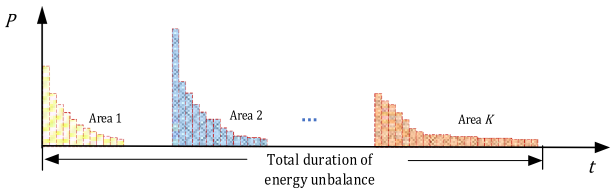

Fig. 5. The normalized power demand in the planning year.

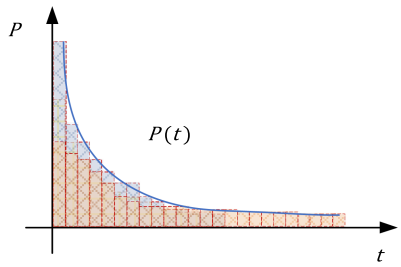

Fig. 6. The power demand graph in the planning year.

0, as shown in Fig. 6. The envelope curve can be obtained, i.e., the characteristic function $P(t)$.

Based on the yearly simulation data, the characteristics of the power demand can be quantified, and the characteristic function $P(t)$ can be obtained.

B. Modeling of Uncertainty

To consider the uncertainty of the integrated renewable energy sources and loads, the proposed demand quantification method is further modified based on the Monte-Carlo simulation. It is effective to model uncertainty by generating numerous random samples and simultaneously modeling multiple uncertain parameters. The detailed demand quantification process is as follows.

1) Obtain the planning scheme for power generation such as coal, photovoltaic (PV), wind turbines (WT), gas, biomass, etc.
2) Based on the Monte-Carlo method, a normal distribution is carried out to simulate uncertain parameters such as the operation curves of PV, WT, and load. The parameters of the normal distribution are set according to experience. A data set of uncertain parameters can be obtained. The data set can be defined as $\{U|u_1, u_2, \ldots u_m, \ldots u_M\}$.
3) Conduct the production simulation with a group of uncertain parameters u_m, and export the hourly operation data.
4) According to the demand quantification method mentioned in Section II-A, the power demand can be quantified.

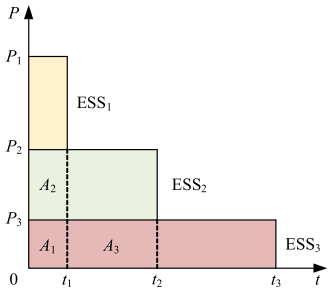

Fig. 7. The coupled relationship of HESS.

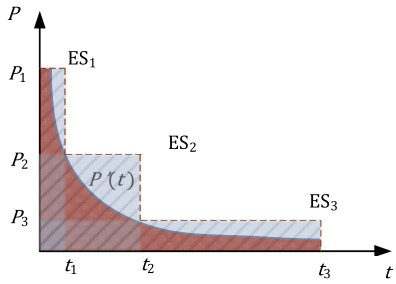

Fig. 8. The matched HESS capacity with the power demand.

5) Set $u_m = u_{m+1}$, and repeat process 3) - 5).
6) Obtain M group of power demand data, and stack them together like Fig. 6.
7) Calculate the probability of each power shortage value.
8) Set a probability threshold θ and acquire the envelope curve $\leq \theta$ and characteristic function $P'(t)$ by data fitting. The probability threshold θ is the scale of the power unbalance that could not be covered by the HESS. Thus, the smaller the threshold, the smaller the power imbalance, but the investment in the energy storage system increases, leading to poorer economic efficiency.

The function $P'(t)$ represents the power demand characteristic of the power system with uncertainty.

III. Planning Model for HESS

According to the characteristic function, the planning model for HESS is proposed in this Section.

A. Graphical Model of HESS

The energy storage capacity and time length are the main variables concerned in the planning problem for HESS. Taking the HESS with three types of energy storage as an example, its coupling relationship is shown in Fig. 7.

In Fig. 7, t_1, t_2, t_3 respectively denote timescales of the three ESS. Each area represents the capacity of different types of energy storage. $(P_1 - P_2)$, $(P_2 - P_3)$ and P_3 represent the power-scales of the three ESS, respectively. The yellow area represents the capacity of ESS_1, not $(0,0) - (0,P_1) - (t_1,P_1) - (t_1,0)$. This is because of that the latter leads to overlap and waste of energy storage capacity across different time scales. Similarly, the green area represents the capacity of ESS_2. The pink area represents the capacity of ESS_3.

Area A_2 denotes the coupled capacity of ESS_2 with ESS_1. Similarly, the area $A_1 + A_3$ denotes the coupled capacity of ESS_3 with ESS_2. The area A_1 denotes the coupled capacity of ESS_3 with ESS_2 and ESS_1. The coupling parts generally belong to ESS with a longer time scale, that can be dispatched to support the operation of ESS with a shorter time scale.

B. Planning Model for Energy-energy ESS

Generally, the energy balance is already taken into consideration in the planning scheme. It is rational to assume that the energy can be balanced in the planning year. Thus, by adjusting the area of HESS considering the investment cost, the power demand can be covered as shown in Fig. 8.

The planning objective is to minimize the investment cost of HESS while satisfying the power demand of the new power system. The objective function F can be formulated according to (1).

$$\min F = \sum_{i=1}^{N-1} C_i \left(P_i - P_{i+1}\right) t_i \; + C_N P_N t_N \tag{1}$$

where N is the number of types of energy storage. C_i denotes the investment cost per unit power-scale of energy storage type i. P_i represents the power-scale of energy storage type i.

The constraints are as follows.

$$P'\left(t_i\right) \leq P_{i+1}, i \in [1, N-1] \tag{2}$$

$$P'\left(1\right) \leq P_1 \tag{3}$$

$$t_i < t_{i+1}, i \in [1, N-1] \tag{4}$$

$$t_{\min} < t_1, \; t_N < t_{\max} \tag{5}$$

$$t_i \in Z^+, i \in [1, N-1] \tag{6}$$

where $P'(\cdot)$ denotes the characteristic function. $t_{\min}$ and $t_{\max}$ are the minimum and maximum value of t_i. $t_i \in Z^+$ means t_i is an integer. Constraints (2)–(6) limit the ranges of optimization variables.

The proposed planning model can be efficiently solved by commercial solution tools. Based on the graphical analysis, the number of variables of the planning model is reduced greatly compared with that of conventional planning methods.

C. Planning Model for Power-energy ESS

Addressing issues of rapid fluctuation and randomness of RES, this section proposes an optimization configuration method for power-energy ESS.

Empirical Mode Decomposition (EMD) is a method for processing non-stationary and nonlinear signals. EMD extracts Intrinsic Mode Functions (IMFs) [19] through a process known as "sifting", which requires that the number of extrema and the number of zero-crossings in an IMF must be equal or differ at most one. Moreover, the meaning of the upper and lower envelopes defined by the local extrema should be zero. The decomposition process is as follows:

1) $x(t)$ is defined to denote the renewable energy output $P^{\mathrm{RES}}t$. Identify the extreme points of $x(t)$ and use spline

interpolation to construct its upper envelope line $E^{\mathrm{U}}(t)$ and lower envelope line $E^{\mathrm{L}}(t)$.

2) Calculate the mean value $\Lambda_\lambda(t)$ of the upper and lower envelope lines. And subtract $\Lambda_\lambda(t)$ from the $x(t)$ to obtain the intermediate signal $h_\lambda^k(t)$.

$$\Lambda_\lambda\ (t) = \ 0.5 * \left[E^{\mathrm{U}}\ (t) + E^{\mathrm{L}}\ (t)\right] \tag{7}$$

$$h_\lambda^k\ (t) = \ x(t) - \Lambda_\lambda\ (t) \tag{8}$$

where λ is the order index of IMF, and k is the index of the iteration number of intermediate signal $h_\lambda^k(t)$.

3) Determine whether $h_\lambda^k(t)$ meets the IMF decision criteria. If it does, set $h_\lambda^k(t)$ as the m order modal component of the IMF. If it does not, repeat steps 1) and 2) using $h_\lambda^k(t)$ as the initial signal, and iterate until the criteria is met.

$$P_\lambda^{\mathrm{IMF}}\ (t) = h_\lambda^k\ (t) \tag{9}$$

4) Calculate the residue $P_\lambda^r(t)$.

$$P_\lambda^r\ (t) = \ x(t) - P_\lambda^{\mathrm{IMF}}\ (t) \tag{10}$$

5) Repeat decomposition, set the residue as the initial signal and repeat the above process until the order M residue cannot extract components that meet the standard.

Finally, the function $P^{\mathrm{RES}}(t)$ is decomposed into several satisfying $P_\lambda^{\mathrm{IMF}}(t)$. And the remaining term $P_\Lambda^{\mathrm{r}}(t)$ is obtained, expressed in (11).

$$P^{\mathrm{RES}}\ (t) = \sum_{\lambda=1}^{\Lambda} P_\lambda^{\mathrm{IMF}}\ (t)\ + P_\Lambda^{\mathrm{r}}\ (t) \tag{11}$$

The EMD method decomposes the original signal $x(t)$ to obtain a series of IMFs, each representing the fluctuation patterns of different time scales, which contain important time-frequency information of the signal. Generally, IMFs exhibit a trend from high frequency to low frequency as the order increases. By reconstructing the IMF components, high-frequency fluctuation information and low-frequency steady-state information can be obtained.

$$P^{\mathrm{H}}\ (t) = \sum_{\lambda=1}^{i} P_\lambda^{\mathrm{IMF}}\ (t) \tag{12}$$

$$P^{\mathrm{L}}\ (t) = \sum_{\lambda=i+1}^{M} P_\lambda^{\mathrm{IMF}}\ (t)\ + P_\lambda^{r}\ (t) \tag{13}$$

$$P^{\mathrm{RES}}\ (t) = P^{\mathrm{H}}\ (t) + P^{\mathrm{L}}(t) \tag{14}$$

where $P^{\mathrm{H}}(t)$ represents the high-frequency fluctuation information of $P^{\mathrm{RES}}(t)$. $P^{\mathrm{L}}(t)$ is the low-frequency steady-state information.

The power-energy ESS can be configured with the high-frequency fluctuation information, which contributes to suppression of power fluctuations for RES. And the capacity of energy-energy ESS can be calculated with the low-frequency steady-state information to achieve within-day peak shaving for RES.

For power-energy HESS, the objective is to reduce the high-frequency fluctuations of the renewable energy station while minimizing the investment, operating costs, and opportunity compensation costs of the supercapacitor. The investment and operating cost $F^{\mathrm{ESS\_SC}}$ are shown in (15), and the opportunity compensation cost F^{B} is shown in (20).

$$F^{\mathrm{ESS\_SC}} = C^{\mathrm{ESS\_SC}}\ E^{\mathrm{ESS\_SC}} \frac{r(1+r)^Y}{(1+r)^Y - 1} + C^{\mathrm{OPER\_SC}} \sum_{t\ =\ 1}^{\mathrm{T}} P_t^{\mathrm{ESS\_SC}} \Delta t_0 \tag{15}$$

where $C^{\mathrm{ESS\_SC}}$ is the investment cost coefficient for the power-energy HESS capacity, $E^{\mathrm{ESS\_SC}}$ is the configured capacity of the power-energy HESS, r is the discount rate, taken as 5%, Y is the operating period, taken as 15 years, $C^{\mathrm{OPER\_SC}}$ is the operating cost coefficient for the power-energy HESS, T is the total number of periods within the system's operating cycle, $P_t^{\mathrm{ESS\_SC}}$ is the power of the power-energy HESS at time t and Δt_0 is the duration of each time period.

If the fluctuation of the high-frequency component is significant and energy storage cannot fully smooth it out, the system must coordinate with other flexible resources for regulation, leading to an increase in system operating costs. Therefore, to measure the increased operating costs due to the high-frequency fluctuations of renewable energy, the opportunity compensation cost is introduced. Its mathematical description is as follows:

$$F^{\mathrm{B}} = \sum_{t=1}^{\mathrm{T}} C^{\mathrm{B}} \left|P_t^{\mathrm{UN}}\right| \Delta t_0 \tag{16}$$

$$P_t^{\mathrm{UN}} = P_t^{\mathrm{ESS\_SC}}\ - P_t^{\mathrm{H}} \tag{17}$$

where C^{B} is the opportunity compensation cost coefficient, P_t^{UN} is the under-compensation amount at time t, and P_t^{H} represents the high-frequency component of the renewable energy power at time t.

The constraints are as follows.

$$0 \le S_t^{\mathrm{ESS\_SC}} \le S_{\max}^{\mathrm{ESS\_SC}} \tag{18}$$

$$0 \le P_t^{\mathrm{ESS\_SC,ch}} \le P_{\max}^{\mathrm{ESS\_SC,ch}} \tag{19}$$

$$0 \le P_t^{\mathrm{ESS\_SC,dis}} \le P_{\max}^{\mathrm{ESS\_SC,dis}} \tag{20}$$

$$S_t^{\mathrm{ESS\_SC}} = S_{t-1}^{\mathrm{ESS\_SC}}\ + \left(\eta^{\mathrm{ch}} P_t^{\mathrm{ESS\_SC,ch}} - \frac{P_t^{\mathrm{ESS\_SC,dis}}}{\eta^{\mathrm{dis}}}\right) \Delta t_0 \tag{21}$$

where $S_t^{\mathrm{ESS\_SC}}$ is the supercapacitor capacity at time t, $S_{\max}^{\mathrm{ESS\_SC}}$ is the upper limit of the supercapacitor capacity, $P_t^{\mathrm{ESS\_SC,ch}}$ is the supercapacitor charging power at time t, $P_{\max}^{\mathrm{ESS\_SC,ch}}$ is the upper limit of the supercapacitor charging power, $P_t^{\mathrm{ESS\_SC,dis}}$ is the supercapacitor discharging power at time t, $P_{\max}^{\mathrm{ESS\_SC,dis}}$ is the upper limit of the supercapacitor discharging power, and η^{ch} and η^{dis} are the charging and discharging efficiencies, respectively.

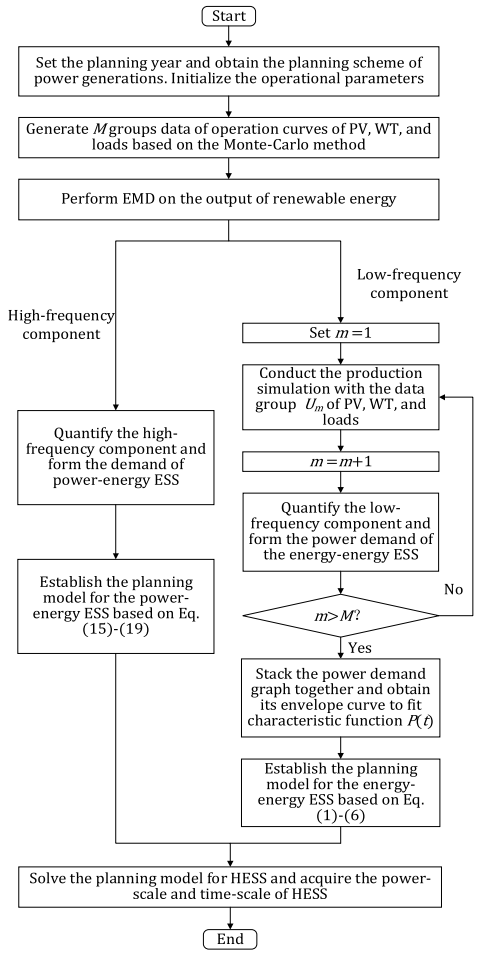

Fig. 9. Flowchart of the proposed data-driven planning method.

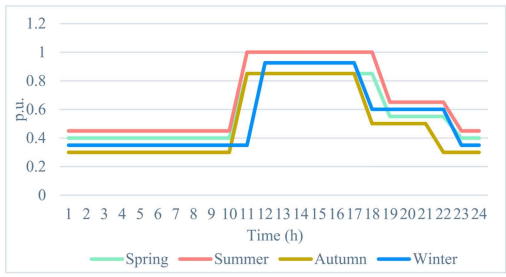

Fig. 10. Export power curve of loads.

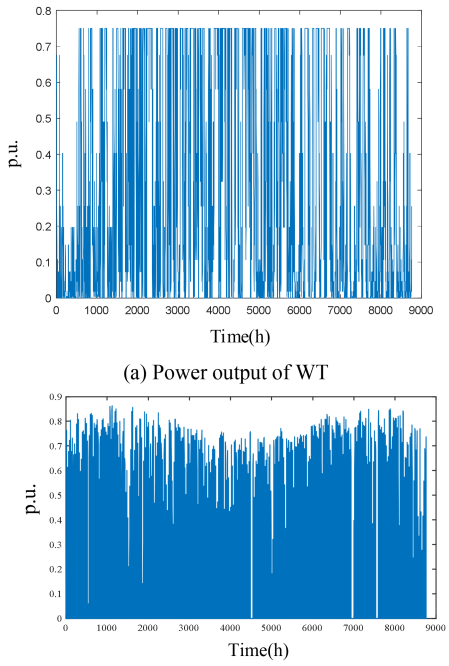

Fig. 11. Power output of WT and PV.

D. Implementation

The flowchart of the proposed data-driven voltage-predictive control is shown in Fig. 9.

First, set the planning year, obtain the planning scheme of power generation, and initialize the operational parameters. Second, simulate the uncertain parameters such as the operation curves of PV, WT, and load based on the Monte Carlo method. Then, conduct the production simulation with multiple uncertain parameters to quantify the power demand of the new power system with a characteristic function. Finally, establish the planning model of energy-energy ESS and power-energy ESS. Finally, the optimal capacity combination can be found.

IV. Case Studies and Analysis

In this section, an under-planning regional-level new power system is adopted as the test case, including the RES, HESS, and a gas power plant. The code is based on MATLAB. The solvers are YALMIP and CPLEX. The time scale of energy-energy ESS is at the hour level, while that of power-energy ESS is at the minute level. The CPU is Intel(R) Core (TM) i9-14900 K @3.20 GHz and the memory is 16 GB. The operating system is Windows 11.

A. Case Overview

In the tested new power system, the maximum load is 8 MW, and the load curve is shown in Fig. 10. The local WT and PV output curves are shown in Fig. 11. According to the local resource conditions, the upper limit of installed capacity for WT, PV and the gas plant is 6.6, 16.5 and 5 MW, respectively.

B. Configuration of RES Capacities

As the new power system is under planning, all these components need to be planned simultaneously and rationally.

First, the optimization analysis of configuration ratios for wind turbines WT, PV is performed. The objective function is to minimize the deviation between the renewable energy output and the load curve.

$$\min f = \sum_{t=1}^{T} |P_{\text{RES}}[t] - P_{\text{load}}[t]| \tag{22}$$

$$P_{\text{RES}}[t] = C_{\text{PV}} * p_{\text{PV}}[t] + C_{\text{WT}} * p_{\text{WT}}[t] \tag{23}$$

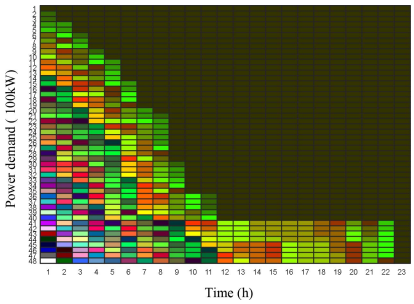

Fig. 12. Demand of regulatory resources.

where T represents the total duration of the renewable energy and load curves, $P_{\text{RES}}[t]$ denotes the total renewable energy output at time t, and $P_{\text{load}}[t]$ signifies the total load at time t. The variables C_{PV} and C_{WT} are variables representing the installed capacities of PV and WT, respectively. $p_{\text{PV}}[t]$ and $p_{\text{WT}}[t]$ indicate the per-unit outputs of the PV and WT at time t, respectively.

The constraints consider the range of installed capacities for PV and WT.

$$0 < C_{\text{PV}} < C_{\text{PV,max}} \tag{24}$$

$$0 < C_{\text{WT}} < C_{\text{WT,max}} \tag{25}$$

where $C_{\text{PV,max}}$ and $C_{\text{WT,max}}$ represent the maximum allowable installed capacities for PV and WT systems, respectively.

By solving the above model, the optimal capacities for the renewable energy can be determined. The resulting capacities of WT and PV are 4.3 MW and 10 MW, respectively.

C. Configuration of Energy-energy ESS With Gas Power Plant

Based on the WT and PV capacities, a production simulation is performed to obtain the moments and information of system power shortages. This data forms the basis for optimizing the capacities of regulatory resources.

Note that, the gas plant can be considered as a regulatory resource, the coupling relationship between HESS and the gas plant can be illustrated as Fig. 7. The objective function of the optimization configuration model is calculated according to (26), with the remaining constraints as given in (2)–(6).

$$\min F = \sum_{i=1}^{N-1} C_i \left(P_i - P_{i+1}\right) t_i \; + C_N P_N t_N + \sum_{i=1}^{N} C_{\text{gas}} P_{\text{gas}} t_i + \sum_{i=1}^{N} D_{\text{gas}} Q_{\text{gas}} t_i \tag{26}$$

where C_{gas} is the investment cost per unit of power generation capacity for the gas plant. P_{gas} represents the power capacity of the gas plant. D_{gas} denotes the operating costs of the gas plant. Q_{gas} indicates the power generation output of the gas plant.

Using the method described in Section III-B, the demand for regulatory resources including gas power plant and HESS by the new power system is determined, as shown in Fig. 12.

Considering that the comprehensive cost of the gas plant is lower than that of HESS, priority is given to using gas power as a regulatory resource to meet the long-term peak electricity demand. The operating parameters of the gas plant include unit capacity investment cost of 2500 CNY/kW and electricity cost of 0.204 CNY/kW. The remaining regulatory demand is met through electrochemical energy storage, with a unit capacity investment cost of 1500 CNY/kW. Based on the method described in Section III-B, the configuration results of regulatory resources are obtained as shown in Table I.

TABLE I
CONFIGURATION OF REGULATORY RESOURCES

	Gas plant	Energy storage system
Capacity	4.2MW	0.9MW/2h 0.2 MW/4h

TABLE II
COMPARISON OF RESULTS

	Scheme 1	Scheme 2	Scheme 3
Utilization rate of renewable energy	91.8%	91.7%	92.1%
Proportion of electricity from renewable energy	66.1%	57.3%	53.4%
Proportion of electricity from the main grid	1.09%	0.85%	1.11%
Average electricity cost (CNY)	0.279	0.288	0.280

To demonstrate the effectiveness of the proposed capacity configuration method, two capacity configuration schemes are selected for comparative analysis.

Scheme 1: The capacity configuration scheme obtained from the method described in this section, including both renewable energy and regulatory resources.

Scheme 2: The installed capacity for WT, PV and the gas plant is 3.6, 8 and 4 MW, respectively. The capacity of HESS is 2.5 MW/h.

Scheme 3: The installed capacity for WT, PV and the gas plant is 3, 7.5 and 4 MW, respectively. The capacity of HESS is 1.7 MW/h.

As for configuration of energy-energy ESS with the gas power plant, the key indicators in this method and the control groups are analyzed, such as the utilization rate of renewable energy, the proportion of electricity from renewable energy, the proportion of electricity from the main grid, and the average electricity cost, as shown in Table II. The results indicate that the configuration scheme obtained by this method is similar to previous schemes.

D. Configuration of Power-energy ESS

According to the method described in Section III-C, the capacity of the power-energy ESS can be calculated, which is determined to be 241.79 kWh. Fig. 13 illustrates the power-energy HESS demand. Then, the configuration results for the capacity and duration of the power-energy ESS can be obtained in Table III.

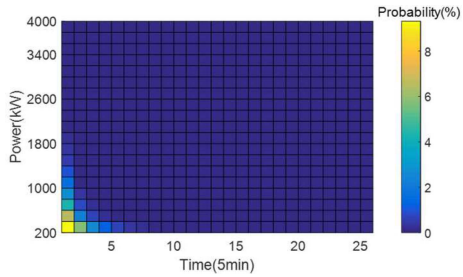

Fig. 13. Demand of power-energy ESS.

TABLE III
CONFIGURATION OF POWER-ENERGY ESS

	5 min	10 min
Capacity	75.12 kWh	166.67 kWh

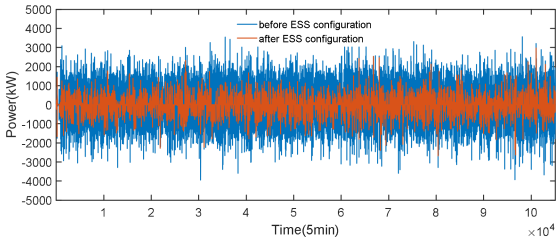

Fig. 14. High-frequency component before and after annual power-energy ESS configuration.

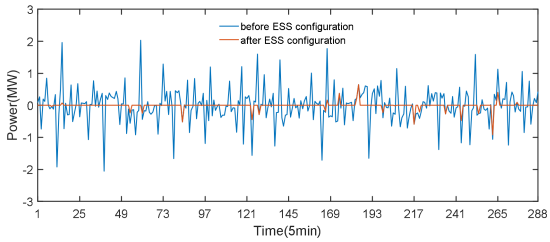

Fig. 15. High-frequency component before and after power-energy ESS configuration on a certain day.

TABLE IV
OPTIMIZATION EFFECT ON THE HIGH-FREQUENCY COMPONENT

Metrics	Before	After	Percentage reduction
the maximum 5-minute fluctuation	6.1749 MW	2.9697 MW	51.91%
the maximum 5-minute negative fluctuation	3.9481 MW	2.6759 MW	32.22%

The fluctuation of low-frequency and high-frequency components before and after configuration is shown in Fig. 14. The high-frequency component before and after the configuration of the power-energy ESS on a certain day is illustrated in Fig. 15.

As for configuration of power-energy ESS, the optimization effect on the high-frequency component is shown in Table IV. It can be observed that after configuration using the proposed optimization method, the maximum 5-minute fluctuation decreased by 51.91%, and the maximum 5-minute negative fluctuation decreased by 32.22%. The high-frequency fluctuation of renewable energy has significantly decreased, demonstrating the effectiveness of the strategy proposed in this paper in smoothing the output fluctuations of renewable energy.

V. CONCLUSION

A lightweight data-driven planning method is proposed for HESS, which is applicable to decoupled operation and planning stages. Different from the conventional multi-stage planning method, the proposed study provides a unique view of the planning problem of HESS. The demand function of the power system with uncertainty is quantified for HESS based on data from the production simulation. The multi-time scale characteristic of HESS is described by a graphical model. Then, a lightweight data-driven planning model with the decoupled operation and planning stage is proposed to optimize the capacities of HESS. Case studies illustrate that the proposed lightweight data-driven planning method can provide a rational configuration scheme for HESS.

Three aspects of studies can be carried out in future research. 1) Adaptively adjust the operating parameters of the algorithm to improve the performance of the proposed method. 2) Accurately quantify the uncertainties of renewable energy and load is crucial. 3) Considering the different operation characteristics between ESS, the selection of technologies routines of HESS is worthy of future research. 4) The function of HESS can be further considered, including market participation, peak shaving, etc. 5) Since this work has proposed a general paradigm, the application in the integrated energy system is promising for further study.

REFERENCES

[1] Y. Wei et al., "Policy and management of carbon peaking and carbon neutrality: A literature review," *Engineering*, vol. 14, pp. 52–63, 2022.
[2] J. Yang et al., "Real-time D-PMU data compression for edge computing devices in digital distribution networks," *IEEE Trans. Power Syst.*, vol. 39, no. 4, pp. 5712–5725, Jul. 2024.
[3] B. Mohandes, M. S. El Moursi, N. Hatziargyriou, and S. E. Khatib, "A review of power system flexibility with high penetration of renewables," *IEEE Trans. Power. Syst.*, vol. 34, no. 4, pp. 3140–3155, Jul. 2019.
[4] M. Sepehry, M. H. Kapourchali, V. Aravinthan, and W. Jewell, "Robust day-ahead operation planning of unbalanced microgrids," *IEEE Trans. Ind. Inform.*, vol. 15, no. 8, pp. 4545–4557, Aug. 2019.
[5] A. Castillo and D. F. Gayme, "Grid-scale energy storage applications in renewable energy integration: A survey," *Energy Convers. Manage.*, vol. 87, pp. 885–894, 2014.
[6] S. Zhang, Y. Mishra, and M. Shahidehpour, "Utilizing distributed energy resources to support frequency regulation services," *Appl. Energ.*, vol. 206, pp. 1484–1494, 2017.
[7] P. Yu et al., "Construction method of ancillary emergency backup service based on battery energy storage system," *Int. J. Elec. Power.*, vol. 147, 2023, Art. no. 108881.
[8] R. Hemmati, H. Saboori, and M. A. Jirdehi, "Stochastic planning and scheduling of energy storage systems for congestion management in electric power systems including renewable energy resources," *Energy*, vol. 133, pp. 380–387, 2017.
[9] R. Hemmati, "Optimal design and operation of energy storage systems and generators in the network installed with wind turbines considering practical characteristics of storage units as design variable," *J. Cleaner Prod.*, vol. 185, pp. 680–693, 2018.

[10] B. Zhao et al., "Tri-level robust planning-operation co-optimization of distributed energy storage in distribution networks with high PV penetration," *Appl. Energy*, vol. 279, 2020, Art. no. 115768.
[11] Z. Zhang et al., "A review of technologies and applications on versatile energy storage systems," *Renew. Sust. Energy Rev.*, vol. 148, 2021, Art. no. 111263.
[12] U. Manandhar, N. R. Tummuru, S. K. Kollimalla, A. Ukil, G. H. Beng, and K. Chaudhari, "Validation of faster joint control strategy for battery- and supercapacitor-based energy storage system," *IEEE Trans. Ind. Electron.*, vol. 65, no. 4, pp. 3286–3295, Apr. 2018.
[13] S. Mohseni et al., "Strategic design optimisation of multi-energy-storage-technology micro-grids considering a two-stage game-theoretic market for demand response aggregation," *Appl. Energy*, vol. 287, 2021, Art. no. 116563.
[14] R. Hemmati, M. Shafie-Khah, and J. P. S. Catalao, "Three-level hybrid energy storage planning under uncertainty," *IEEE Trans. Ind. Electron.*, vol. 66, no. 3, pp. 2174–2184, Mar. 2019.
[15] X. Shen et al., "Optimal hybrid energy storage system planning of community multi-energy system based on two-stage stochastic programming," *IEEE Access*, vol. 9, pp. 61035–61047, 2021.
[16] Y. Wang et al., "Research on capacity planning and optimization of regional integrated energy system based on hybrid energy storage system," *Appl. Therm. Eng.*, vol. 180, 2020, Art. no. 115834.
[17] F. Yang, Z. Zhang, G. Li, Y. Liu, and L. Zhang, "Hybrid energy storage planning method based on benders decomposition and wavelet analysis," in *Proc. IEEE Sustain. Power Energy Conf.*, 2021, pp. 1262–1266.
[18] Y. Huo, Z. Wu, J. Dai, W. Duan, and J. Jiang, "Lightweight data-driven planning method for hybrid energy storage systems," in *Proc. IEEE/IAS Ind. Commercial Power System Asia*, 2023, pp. 1831–1836.
[19] T. Yuan et al., "Optimal allocation of power electric-hydrogen hybrid energy storage of stabilizing wind power fluctuation," *Proc. CSEE*, vol. 44, no. 4, pp. 1397–1406, 2023.